



Published in final edited form as:

*Nat Methods*. 2020 February ; 17(2): 175–183. doi:10.1038/s41592-019-0687-1.

## BIOPHYSICAL PREDICTION OF PROTEIN-PEPTIDE INTERACTIONS AND SIGNALING NETWORKS USING MACHINE LEARNING

Joseph M. Cunningham<sup>1</sup>, Grigoriy Koytiger<sup>1,2</sup>, Peter K. Sorger<sup>1,†</sup>, Mohammed AIQuraishi<sup>1,\*†</sup>

<sup>1</sup>Laboratory of Systems Pharmacology, Department of Systems Biology, Harvard Medical School, Boston, Massachusetts, USA

<sup>2</sup>Current Address: cascade.bio, Cambridge, Massachusetts, USA

### Abstract

In mammalian cells, much of signal transduction is mediated by weak protein-protein interactions between globular peptide-binding domains (PBDs) and unstructured peptidic motifs in partner proteins. The number and diversity of these PBDs (over 1,800 are known), low binding affinities, and sensitivity of binding properties to minor sequence variation represent a substantial challenge to experimental and computational analysis of PBD specificity and the networks PBDs create. Here we introduce a bespoke machine learning approach, hierarchical statistical mechanical modelling (HSM), capable of accurately predicting the affinities of PBD-peptide interactions across multiple protein families. By synthesizing biophysical priors within a modern machine learning framework, HSM outperforms existing computational methods and high-throughput experimental assays. HSM models are interpretable in familiar biophysical terms at three spatial scales: the energetics of protein-peptide binding, the multi-dentate organization of protein-protein interactions, and the global architecture of signaling networks.

### INTRODUCTION

Signal transduction downstream of transmembrane receptors, particularly receptor tyrosine kinases (RTKs), is commonly mediated by networks of weak protein-protein interactions (PPIs) having dissociation constants in the micromolar range.<sup>1,2</sup> Many such interactions

---

Users may view, print, copy, and download text and data-mine the content in such documents, for the purposes of academic research, subject always to the full Conditions of use:[http://www.nature.com/authors/editorial\\_policies/license.html#terms](http://www.nature.com/authors/editorial_policies/license.html#terms)

\*Address correspondence to: Mohammed AIQuraishi, WAB 438, Harvard Medical School, 200 Longwood Avenue, Boston MA 02115, Tel: 617-432-6901, [alquraishi@hms.harvard.edu](mailto:alquraishi@hms.harvard.edu).

<sup>†</sup>These authors contributed equally.

#### AUTHOR CONTRIBUTIONS

JMC, PKS, and MA conceived and designed the model, analysis and computational experiments. JMC implemented model and carried out the analysis and experiments. GK collected and processed binding and structural data and contributed to the analysis. All authors wrote and reviewed the manuscript.

#### COMPETING INTERESTS

PKS is a member of the SAB or Board of Directors of Merrimack Pharmaceutical, Glencoe Software, Applied Biomath and RareCyte Inc. and has equity in these companies; Sorger declares that none of these relationships are directly or indirectly related to the content of this manuscript.

involve peptide-binding domains (PBDs; e.g. SH2, SH3, PDZ domains) that bind short linear sequences in partner proteins (hereafter “peptides” or “peptidic sites”) to form multi-protein scaffolds and regulate enzyme activities.<sup>3–6</sup> Oncogenic mutations are common in PBD-containing proteins and many of these proteins are drug targets.<sup>7,8</sup> The large number of PBDs and peptidic sites presents a considerable hurdle to structural understanding: PBDs and peptidic sites are too numerous for comprehensive crystallization or analysis by cryo-EM.<sup>9–11</sup>

The low affinities of PBD-mediated interactions represents a second challenge to their characterization: relatively few PBD-peptide complexes are detectable using the pull-down assays from cell extracts currently being performed on large scale, and this has necessitated the use of other methods such as protein-peptide arrays, isothermal titration calorimetry, and surface plasmon resonance.<sup>12–15</sup> Such methods require synthetic and/or immobilized peptides and recombinant proteins and do not readily scale to a full proteome; as a result, binding data on many PBD families remain sparse. Computational approaches have been stymied by this data scarcity and by the diversity of PBD folds. Consequently, modeling efforts to date have focused primarily on individual domains (e.g. the SH2 domain of the protein STAP1)<sup>16–19</sup> or domain families for which sufficient binding data are available (e.g. all SH2 domains)<sup>20</sup>.

In this paper we describe a machine learning method, hierarchical statistical mechanical modelling (HSM), for studying PBD-peptide interactions *en masse*. HSM uses experimental domain-peptide array data to model PPIs by generalizing along two axes: from individual PBD-peptide interactions to multi-dentate PPIs, and from one PBD family to another. A key feature of HSM is the inference of a unified energy model that enables transfer of biochemical and structural knowledge from domain families for which abundant binding data are available (e.g. SH2 domains) to ones for which data are sparse (e.g. PTB domains). We show that HSM predicts PBD-peptide biophysics with precision and recall superior to existing computational methods and to high-throughput assays (e.g. protein arrays, yeast two-hybrid screening, and affinity mass spectrometry). By exploiting biophysical knowledge, machine learning, and large-scale but sparse empirical data, HSM provides a substantial technical and biological advance in the study of PBDs and the cellular signaling networks they form in both physiological and dysregulated conditions.

## RESULTS

### Model design and approach

We constructed HSM models for six common PBD families involving phosphotyrosine, polyproline, and C-terminal peptidic sites (PDZ, SH2, SH3, WW, WH1, PTB; n = 823 domains) and for tyrosine kinases and protein tyrosine phosphatases (TK, PTP; n = 143 domains; Fig. 1a; Supplementary Table 1). In the human proteome, the total number of PBD-containing proteins is estimated to be  $\sim 10^4$  proteins (Fig. 1b) which participate in  $\sim 10^5$  -  $10^6$  interactions (Fig. 1c). The eight domains studied in this paper constitute  $\sim 39\%$  of the total number of human PBDs (see Supplementary Note 1). In principle, the same modeling framework is applicable to all remaining human PBDs, but a scarcity of data (<100 reported interactions per family) makes it difficult to evaluate model performance.

HSM is a method for inferring structured Hamiltonians, the mathematical function that maps the state of a system to its energy and, consequently, to its thermodynamic properties. In classical statistical mechanics, this function is derived from physical theory. In HSM, an empirical approximation to the Hamiltonian is machine-learned in a manner that satisfies known and inferred biophysical constraints (see Supplementary Note 2). Due to data limitations, the process of inferring full Hamiltonians is underdetermined. Consequently, the HSM model is more appropriately termed a pseudo-Hamiltonian. We constrain the model to include only energy terms corresponding to single residues and interactions between pairs of residues, one in the domain and one in the peptide. Given additional data, higher-order effects (e.g. steric effects of triplets of residues) could be added to the model to more completely approximate the true Hamiltonian.

Prior to initiating machine learning we carry out a combined sequence/structure alignment that brings into correspondence all residue positions of a given PBD family and peptide class, resulting in a unified system of residue coordinates. HSM then learns a pseudo-Hamiltonian that maps individual residues and residue pairs to binding energies in a manner that respects two constraints: (i) within a PBD family, a residue or residue pair at the same position always contributes the same energy and, (ii) across PBD families, residue pair energies are derived from a fixed pool of energy potentials.

The first constraint is motivated by atomic-resolution structures of PBD-peptide co-complexes. These complexes show that structurally aligned residue positions in a domain family create biophysically similar binding pockets (Supplementary Fig. 1)<sup>6,13,21–24</sup>. Thus, learned energies for a given residue position should be transferable among domains from the same PBD family. Models applicable to all domains in one PBD family are described below as *HSM for Independent Domains* (HSM/ID) (Fig. 1d). HSM/ID is a generalization of the multiscale statistical mechanical (MSM)<sup>20</sup> model we previously used to model SH2 domains. However, unlike MSM, HSM/ID does not require alignment on phosphotyrosine sites (the chemical moiety recognized by all SH2 domains) or high-resolution protein structures.

The second constraint is motivated by our analysis of residue-residue potentials learned by HSM/ID, which revealed similar energetic patterns for groups of residues across families of domains (Supplementary Fig. 2). Such similarity is consistent with the view that interactions among diverse types of proteins are mediated by a relatively limited set of interaction surfaces.<sup>25,26</sup> We formalize this observation by forcing the HSM model to learn a shared set of residue-residue potentials that are assigned via a learned weighted mixture to specific position pairs in each PBD family (Fig. 1e). We find that a small number of potentials used in combination can capture the observed set of sterically and chemically distinct interaction surfaces, enabling information transfer among residue positions. The model that uses shared potentials and satisfies the HSM/ID constraint is referred to as *HSM for Domains* (HSM/D).

## Training and validation

To train HSM models, we assembled a dataset of  $\sim 2 \times 10^6$  PBD-peptide interactions derived primarily from array-based assays; data were binarized to allow values from different experimental methods to be combined, yielding 3-5% positive interactions (Supplementary

Table 1). To evaluate the merits of enforcing different constraints on learned energies we trained eight separate HSM/ID models, one for each PBD/enzyme family, and a single unified HSM/D model covering all families. We are unaware of any single model that covers an entire PBD family (including sequence variants that are associated with disease; our SH2-specific MSM framework is the exception<sup>20</sup>) or PBDs from multiple families (Supplementary Table 2). We therefore compared HSM against conventional position-specific scoring matrices (PSSM<sup>27</sup>) and, when available, previously published machine learning models covering subsets of PBD families.

HSM/D and HSM/ID significantly outperformed existing machine learning models<sup>17,28</sup> ( $p = 6.4 \times 10^{-12}$ ; DeLong test) and PSSMs<sup>27</sup> ( $p = 4.9 \times 10^{-56}$ ; DeLong test) in all cases in which comparison was possible (Fig. 2a; Supplementary Fig. 3a; Supplementary Table 3). We also observed strong concordance between experimentally-derived and model-inferred interaction probabilities (Supplementary Fig. 3b), suggesting that predicted values can be meaningfully interpreted as physical affinities. HSM/D outperformed HSM/ID across all domains ( $p = 2.4 \times 10^{-2}$ ; DeLong test), likely due to information sharing among domains. Improvement was observed for both high-data (*e.g.* PDZ) and low-data (*e.g.* PTB) domains. HSM covers more PBD families and a substantially larger fraction of each family than other methods (parentheses in Fig. 2a). Critically, much of the improvement is concentrated in low false-positive rate (FPR) regions (FPR < 0.10), where realistic use of model predictions would occur.

Many mammalian signal transduction proteins contain multiple PBDs and/or peptidic sites. We modelled multi-dentate PPIs involving multiple peptidic sites and/or PBDs by computing the energies of all possible binding configurations using the HSM/D pseudo-Hamiltonian and then extracting the probability of the bound ensemble. These whole-protein models are referred to as *HSM for Proteins* (HSM/P) (Fig. 1c; Supplementary Table 4). The additivity of Hamiltonians is a key advantage of the HSM approach; it enables the principled aggregation of domain-level predictions while accounting for increases in affinity arising from multi-dentate binding. Thus, HSM/P accounts for cooperativity, but not changes in binding energy associated with steric hindrance at the level of tertiary structure. This limitation may not be consequential since many proteins containing PBDs and peptidic sites involve discrete folded domains separated by structurally disordered and presumably flexible polypeptides.

To evaluate the accuracy of HSM/P models, we constructed a “gold standard” set of 32,504 direct PPIs derived from two curated molecular interaction databases (BioGRID<sup>29</sup>, IntAct<sup>30</sup>) using three criteria: (i) direct interactions, (ii) low-throughput assays, and (iii) multiple verifications (see Methods). We assessed the performance of HSM/P and three recent high-throughput experimental assays<sup>11,31–33</sup> (Supplementary Table 5) against this gold standard set. Because HSM is only trained on domain-peptide interactions, the gold standard protein-level PPI data is independent of HSM predictions. To further guard against data leakage, we removed from the gold standard set any PPIs comprised of domain-peptide interactions present in the HSM training set. To ensure a fair comparison, recall was computed on the subset of PPIs detectable by each method (*e.g.* tested pairs in a yeast two-hybrid binary interactome). At comparable false-discovery rates, HSM/P roughly doubled the recall

achieved by any of the three experimental assays (Fig. 2b). This comparison is likely to underestimate the actual improvement provided by HSM due to (i) underreporting of weak PPIs in the gold standard dataset (these appear as false positive HSM predictions),<sup>1,34</sup> and (ii) the presence in the gold standard dataset of interactions that are mediated by domains other than the modeled PBDs (these appear as false negative HSM predictions). The comparison nonetheless shows that HSM/P improves on high-throughput experimental methods while covering the space of poorly-characterized interactions.

To assess the utility of HSM in predicting novel protein-protein interactions, we combined protein-level data from BioGRID and high-throughput experiments and filtered them for PPIs discovered subsequent to the date HSM domain-level training data were reported (see Methods). Given the number of domain- and peptide-containing proteins in the human proteome for which HSM is capable of making predictions, the highest number of possible PPIs is ~5.3M. At an expected FDR of 0.01 (calibrated using the results of Fig. 2), HSM/P predicts 23,309 PPIs not reported in the combined protein-level data prior to the time of the split. Among these, 161 interactions have subsequently been detected experimentally (Fig. 3; Supplementary Fig. 4); we use HSM/P to gain detailed insight into them. Almost all interactions examined (99%,  $n = 160$  PPIs) involved one or more high-affinity PBD-peptide interactions ( $p < 0.05$ , HSM/D prediction) but they were otherwise diverse: 69 (43%) were multi-dentate (with two or more strongly-interacting PBDs), 11 (7%) involved multiple PBDs from one or more families and a single peptide, and 68 (42%) involved multiple peptides and one PBD. Phosphotyrosine- and proline-binding predominated (Fig. 3), but the two chemistries were largely non-overlapping (only 6 PPIs combined both). In most interactions we also observed either that (i) the number of multiply bound peptidic sites (*i.e.* sites having more than one high-affinity PBD partner) exceeded the number of PBDs ( $n = 106$  PPIs), and/or (ii) that multiple peptidic sites strongly interacted with a single PBD ( $p < 0.05$ , HSM/P;  $n = 119$  PPIs). We expect both types of interactions to decrease off-rates ( $K_{off}$ ) while minimally impacting on-rates ( $K_{on}$ ). Consequently, the affinities of these PPIs should be higher than predicted from PBD-peptide affinities considered individually (that is, they should exhibit cooperativity). Phosphosite-binding has the additional property of being regulable by kinases and phosphatases, further diversifying the properties of multidentate interactions.

### Mechanistic insights into PBD-peptide binding.

How well does HSM capture the details of a PBD-peptide interaction known from a high-resolution structure? To investigate this we examined the structural basis of SH3-peptide binding; similar analyses of other PBD families are shown in Supplementary Fig. 5 and 6. To identify key features in PBD-peptide interaction based on energetic similarity, the Pearson correlation coefficient was calculated for all residue-to-residue energy potentials across domain positions (Fig. 4a) and then used as the basis for hierarchically clustering domain positions. To visualize energetic similarity, the four maximally separated clusters were colored using distinct colors (“anchors” in Fig. 4a, bottom). All other clusters were colored using a weighted mixture of these four colors, with cophenetic distance as the weight (see Methods and Supplementary Fig. 5a for color mixtures). Resulting colors were mapped onto the SH3 domain of HCK, an SH3-peptide co-complex for which a high-

resolution structure is available (PDB:2OI3; Fig. 4b). The canonical SH3 binding pocket is known to involve a conserved triplet of aromatic residues (W114, Y132, Y87) comprising two polyproline type-II (PPII) helix xP-recognition grooves and specificity-defining n-Src and RT-loops<sup>21,35</sup> (Fig. 4b–c). W114 constitutes a “tryptophan switch” that can adapt to support both Class I (N-to-C oriented) and Class II (C-to-N oriented) peptide binding.<sup>36</sup> HSM reveals the involvement of two additional residues in peptide binding (Y89, Y127; Fig. 4d); these residues are energetically similar to W114 (shared green color), potentially contributing to binding energy via van der Waals forces (involving the tryptophan aromatic core) or via hydrogen-bonding (involving the tyrosine alcohol group). Y89 and Y127 appear to function cooperatively with W114 to facilitate binding in Class I and Class II conformations, with Y89 exhibiting features characteristic of both W114 and Y87 (Y89 is darker green, similar to Y87 in Fig. 4b). The existence of such energetic coupling is confirmed by the selectivity of W114 and Y89 for a residue adjacent to the core proline motif on the peptidic site (Fig. 4d, bottom). We also observed energetically similar residues in the RT and n-Src loops (Fig. 4e; shared gold color). This similarity, supported by associated energy profiles (Fig. 4e, bottom), is consistent with the conformational flexibility observed in the peptidic segments adjacent to the RT and n-Src loops (Fig. 4c): all residues in both loops have similar physico-chemical preferences which, in conjunction with their flexibility, allows them to act cooperatively. Thus, even though HSM uses no high-resolution structural information for training, it correctly infers known binding motifs (*e.g.* the W114 tryptophan switch) as well as previously unrecognized aspects of peptide binding (*e.g.* the role of Y89 and Y127 in Class I vs. II binding). We conclude that HSM generates an energy-based description of protein mechanism from which novel biophysical and structural insights can be obtained.

As a second approach to studying the energies that comprise HSM predictions, we mapped predicted interaction energies onto the HCK co-complex (PDB: 2OI3). Residues on the surface of the domain were colored by mean energies of interaction with peptidic residues at defined radii (2.5Å, 5Å, and 10Å) and in total (Fig. 5a). Attractive regions (blue) broadly correspond to known interaction surfaces such as the RT-loop and proline recognition pocket. The peptide bound to HCK in this complex (HSKYPLPPLPSL) is unusual however: it binds in a Class I (N-to-C oriented) conformation involving the typical proline motif (HSKYPLPPLPSL) but an atypical N-terminal sequence (**HSKYPLPPLPSL**).<sup>37,38</sup> HSM predicts a strongly favorable set of interactions for the proline motif involving both the conserved tyrosine residues (Y87, Y132) as well as two adjacent polar residues S130, N131 (Fig. 5b). Although the role of the tyrosine residues is well-described<sup>21,37,38</sup>, the contributions of S130 and N131 are not. We speculate that these residues may serve to decrease off rates by coming into contact with a dissociating peptide.

In its specificity defining N-terminal sequence, the bound peptide is atypical with an aromatic tyrosine residue at the -3 position and a basic lysine residue at the -4 position.<sup>37</sup> Compared to the typical peptide conformation, which smoothly curves into the RT and n-Src pocket, this induces an atypical, “S-shaped” conformation that involves two structural differences: K(-4) is in an orientation that is typically occupied by the -3 position and Y(-3) sterically hinders H93 (Fig. 5c). Despite this unusual arrangement, HSM predicts the



expected energetics: the RT-loop has a broadly attractive interaction with the anchoring basic residue (K(-4) and E94 / D95, possibly electrostatic) along with weaker interactions between H(-6) and Y127, which may involve van der Waals forces. Similarly, HSM assigns repulsive energies to the sterically hindered H93 residue. Speculatively, this unfavorable interaction suggests a potential mechanism for optimizing the binding affinity of the peptides; HSM suggests that smaller, non-polar residues (leucine and isoleucine are the most favorable substitutions) would better enhance affinity at position (-3) than tyrosine.

### Insights into signaling networks.

Many proteins contain multiple PBDs of different classes with and without co-occurring peptidic sites. To study networks involving this type of binding, we generated a proteome-wide node-edge graph of high-confidence human PPI predictions (HSM/P,  $p > 0.7$ ), with nodes corresponding to proteins and edges to interactions (Fig. 6). Networks were laid out using an automated, repulsion-based algorithm that places nodes with similar neighbors nearby (*i.e.* proteins having similar sets of interacting proteins; Methods). We found that proteins containing PBDs from the same family interacted with similar sets of partners, resulting in PBD “neighborhoods” (Supplementary Fig. 7). Globally, the network is further divided into clusters rich in phosphosite-binding and polyproline-binding, with relatively few interconnecting proteins. This hierarchical organization is suggestive of separate, potentially independently-evolving, signaling programs.

Many PBD families form distinct subnetworks (Supplementary Fig. 7), with a broad range of microscale structures such as bifans and feed-forward loops.<sup>39</sup> The existence of common peptidic ‘currencies’ for PBDs based on phosphosite and polyproline binding allows distinct PBD-specific subnetworks to interact, establishing the observed mesoscale structure. We speculate that proteins with PDZ and/or SH3 domains may have evolved to interconnect the phosphosite-binding and polyproline-binding signaling currencies (Fig. 6).

## DISCUSSION

The HSM approach to modeling PBD-mediated interactions represents a form of bespoke machine learning in which statistical mechanical principles and universal features of protein chemistry are wedded to the data-driven learning paradigm through the power of automatic differentiation frameworks (*e.g.* TensorFlow). Bespoke models like HSM combine the robustness of machine learning—with respect to learning from complex, heterogeneous, and incomplete data—with the interpretability of fundamental (bio)physical theory. We speculate that the performance achieved by HSM is unlikely to be possible using a generic machine learning approach.

Because learned pseudo-Hamiltonians are the basis of HSM, it is possible to interpret learned interactions in terms of familiar position-specific binding energies. HSM is therefore able to provide structural insight at three spatial scales: the residue/co-complex level, by facilitating understanding and prediction of PBD and/or peptidic function; the protein level, by quantifying relative contributions of individual PBDs and ligands in multi-dentate interactions; and the network level, by enabling large scale modeling of information transmission from the cell surface to determinants of cell structure and function.

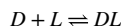
The biophysical detail captured by HSM is most readily illustrated by comparing learned energies to insights inferred from crystal structures, as illustrated in this paper by analysis of SH3 domains, one of the eight classes of PBDs/enzymes we model. We find that HSM provides insight into regions of contact that are remarkably similar to those obtained from crystal structures while also providing a broader synthesis obtainable only from a comprehensive picture of all known SH3 structures.

For well-studied PBD families (SH2, SH3, PDZ) the current work substantially extends current understanding of binding modes and for less well-understood domains (*e.g.* PTB, WH1) it provides new insights. The flexibility of HSM representation makes it adaptable to modeling mutant PBDs and peptides in disease and to designing peptide-based drugs or PBD-like biosensors. In the future it should be possible to develop models for PBDs (*e.g.* BRCT, 14-3-3) that currently lack sufficient data. We expect this to yield comprehensive, proteome-scale models of PBDs in mitogenic and inflammatory signaling and of PBD and peptidic site mutations in diseases such as cancer.

## Online Methods

### HSM - models

We denote a given PBD by  $D$  and its putative cognate peptide by  $L$ , and consider the reaction:



where  $D+L$  represents the pair in an unbound configuration and  $DL$  in a bound configuration. We associate a Hamiltonian with both the unbound,  $\mathcal{H}(D+L)$ , and bound,  $\mathcal{H}(DL)$ , states. We assume that the energies associated with the unbound configuration are additive, *i.e.*  $\mathcal{H}(D+L) = \mathcal{H}(D) + \mathcal{H}(L)$ .

Every Hamiltonian is decomposed into a set of energy functions  $\{\epsilon(\cdot)\}$ , such that each function maps a set of residues (singles or pairs) to an energetic contribution, dependent on the: (i) state of the interaction (bound ( $b$ ) or unbound ( $u$ )), (ii) position(s) of residue(s) in the canonical alignment, and (iii) order of the interaction (singleton or pairwise). We denote the state and position in subscript and the order in a superscript; for example  $e_{b,i,j}^{(2)}$  corresponds to the pairwise (*i.e.*, order 2) interaction between the  $i$ -th PBD position and  $j$ -th peptide position in a bound PBD-peptide complex. A Hamiltonian is then defined by a summation over these energy functions:

$$\mathcal{H}(D) = \sum_{i=1}^{|D|} e_{u,i}^{(1)}(D_i)$$

$$\mathcal{H}(L) = \sum_{i=1}^{|L|} e_{u,i}^{(1)}(L_i)$$



$$\mathcal{H}(DL) = \sum_{i=1}^{|D|} e_{b;i}^{(1)}(D_i) + \sum_{j=1}^{|L|} e_{b;j}^{(1)}(L_j) + \sum_{i=1}^{|D|} \sum_{j=1}^{|L|} e_{b;i,j}^{(2)}(D_i, L_j)$$

In general, a Hamiltonian should be composed of all possible interaction orders (*i.e.* all possible subsets of residues in a complex). Due to limitations in available experimental data, we constrain our representation to first- and second-order interactions. Thus, HSM is more correctly thought of as a pseudo-Hamiltonian. The above model formulation corresponds to a single PBD family in the case of HSM/ID.

A stronger prior can be placed on this pseudo-Hamiltonian by redefining the second-order energy functions to be linear combinations of an underlying basis set shared among all PBD families:

$$e_{b;i,j}^{(2)}(D_i, L_j) = \sum_{k=1}^K w_{i,j}^k \cdot b^k(D_i, L_j)$$

Where  $K$  is the number of basis functions,  $b^k$  is the  $k$ -th basis, and  $w_{i,j}^k$  is a learned weight associating the  $k$ -th basis with position pair  $(i,j)$ . Note that the weights are dependent on position, whereas the basis functions are independent of position and common to all PBDs and all families. This model corresponds to the HSM/D formulation.

Finally, we consider the interaction of two proteins  $\mathcal{P}_1$  and  $\mathcal{P}_2$ :

$$\mathcal{P}_1 + \mathcal{P}_2 = \mathcal{P}_1 \mathcal{P}_2$$

Let  $\beta(\mathcal{P}_1, \mathcal{P}_2)$  define all permissible bound states between the two proteins. A permissible state is a set comprised of PBD-peptide pairs  $\{DL\}$  such that every pair has a non-zero probability of interaction in HSM and no PBD or peptide is paired more than once. For a given bound state  $B \in \beta(\mathcal{P}_1, \mathcal{P}_2)$ , we define the Hamiltonian:

$$\mathcal{H}(B) = \sum_{DL \in B} \mathcal{H}(DL) + \sum_{D \notin B} \mathcal{H}(D) + \sum_{L \notin B} \mathcal{H}(L)$$

While the unbound state Hamiltonian is described by:

$$\mathcal{H}(\mathcal{P}_1 + \mathcal{P}_2) = \sum_{D \in \mathcal{P}_1} \mathcal{H}(D) + \sum_{L \in \mathcal{P}_2} \mathcal{H}(L)$$

### HSM – probabilistic derivation

To learn energy functions, we first translate the model described above into a probabilistic framework.<sup>20</sup> Using the Boltzmann distribution, we write the likelihood of the canonical ensemble ( $ce$ ) representing the bound and unbound states as:

$$p^{(ce)}_{(D+L)} = \frac{1}{Z(D,L)} e^{-\frac{1}{kT}(\mathcal{H}(D) + \mathcal{H}(L) - TS_u)}$$

$$p^{(ce)}_{(DL)} = \frac{1}{Z(D,L)} e^{-\frac{1}{kT}(\mathcal{H}(DL) - TS_b)}$$

where  $Z(D,L)$  is the partition function over the two states:

$$Z(D,L) = e^{-\frac{1}{kT}(\mathcal{H}(D) + \mathcal{H}(L) - TS_u)} + e^{-\frac{1}{kT}(\mathcal{H}(DL) - TS_b)}$$

and  $T$  is the temperature,  $k$  the Boltzmann constant, and  $S_u$  and  $S_b$  are the entropies associated with the unbound and bound states, respectively. Note that entropies are not sequence specific.

Using the same distribution, we define the likelihood of a pair of interacting proteins in configuration  $B$  as

$$p^{(ce)}_{(B)} = \frac{1}{Z(\mathcal{P}_1, \mathcal{P}_2)} e^{-\frac{1}{kT}(\mathcal{H}(B) - T(|N_b(B)| S_b + (|N| - |N_b(B)|) S_u))}$$

where  $N_b(B)$  defines the number of domains in a bound state in configuration  $B$  and  $N$  defines the total number of domains. The partition function over the interacting proteins is consequently defined as:

$$Z(\mathcal{P}_1, \mathcal{P}_2) = e^{-\frac{1}{kT}(\mathcal{H}(\mathcal{P}_1) + \mathcal{H}(\mathcal{P}_2) - T|N| S_u)} + \sum_{B \in \beta(\mathcal{P}_1, \mathcal{P}_2)} e^{-\frac{1}{kT}(\mathcal{H}(B) - T(|N_b(B)| S_b + (|N| - |N_b(B)|) S_u))}$$

Using this probabilistic formulation we can apply machine-learning techniques to learn model parameters.

The above formulation contains an inherent indeterminacy however. Specifically, algebraic simplification yields partition functions that are exclusively described in terms of differences between bound and unbound terms. As a result, the parameters we learn are differences in energy. This is illustrated by simplification to the standard logistic function:

$$p^{(ce)}(DL) = \frac{e^{-\frac{1}{kT}(\mathcal{H}(DL) - TS_b)}}{e^{-\frac{1}{kT}(\mathcal{H}(D) + \mathcal{H}(L) - TS_u)} + e^{-\frac{1}{kT}(\mathcal{H}(DL) - TS_b)}}$$

$$p^{(ce)}(DL) = \frac{e^{-\frac{1}{kT}(\mathcal{H}(DL) - \mathcal{H}(D) - \mathcal{H}(L) - T(S_b - S_u))}}{1 + e^{-\frac{1}{kT}(\mathcal{H}(DL) - \mathcal{H}(D) - \mathcal{H}(L) - T(S_b - S_u))}}$$

Expanding the Hamiltonian, we are left with a function that is a difference of bound and unbound energies:

$$\mathcal{H}(DL) - \mathcal{H}(D) - \mathcal{H}(L) = \sum_{i=1}^{|D|} (e_{b,i}^{(1)}(D_i) - e_{u,i}^{(1)}(D_i)) + \sum_{j=1}^{|L|} (e_{b,j}^{(1)}(L_j) - e_{u,j}^{(1)}(L_j)) + \sum_{i=1}^{|D|} \sum_{j=1}^{|L|} e_{b,i,j}^{(2)}(D_i, L_j)$$

These differences, which we will denote by  $\Delta\mathcal{H}^{(i)}$ , in addition to the change in entropy,  $S$ , are the uniquely determinable values. Hence the inferred energy functions represent the difference in energy associated with binding a peptide. This indeterminacy extends to the protein interaction model described below.

Given a likelihood function, we can define a loss function. Using the negative of the conditional log-likelihood we define the loss function as:

$$Loss := - \left[ p^{(emp)} \log p^{(ce)} + (1 - p^{(emp)}) \log(1 - p^{(ce)}) \right]$$

This function maximizes the conditional likelihood of the data over the available training set. We encourage sparsity via an  $L^1$  regularization penalty. In HSM/ID the penalty is placed on all weights, while in HSM/D the basis sets are excluded.

### HSM/D (independent and universal)

**Data**—Sequences for PBDs were taken from the UniProt database and aligned using the Superfamily<sup>40</sup> Hidden Markov Model (HMM) associated with each PBD's respective fold. Sequences were aligned and trimmed to the model using HMMER3.1b2 (hmmalign and alimask; see Supplementary Data Set 1).

The space of PBDs considered in this work divided naturally into three peptidic types for the purpose of alignment: phosphosites, C-terminal sites and 'other' sites. Phosphosites, bound by the SH2, PTB/PID, TK and PTP families, were aligned using the central phosphorylated residue and trimmed to include the seven leading and trailing residues. C-terminal sites, associated with the PDZ family, were aligned to the C-terminus and trimmed to include the trailing six residues. In both cases, the choice of site length was based on examination of representative crystallographic structures of PBD-peptide co-complexes.

The ‘other’ sites, associated with SH3, WW, and WH1/EVH1 domains, were aligned with reference to PBD-peptide co-complexes. All co-complexes of a given family were extracted from the Protein Data Bank and structurally aligned using a rigid-body alignment<sup>38</sup>, with the PBD domains serving as the reference points (*i.e.* the positions of peptides were ignored when defining the alignment, but were rigidly transformed in the same way as the domain). This alignment induced a structure-based correspondence between peptides, even ones with highly divergent sequences. We extracted a multiple sequence alignment (*i.e.* residue-to-residue correspondences with no internal gaps) from the structural alignment by pairing residues between peptides such that the sum of Euclidean distances between paired residues is minimized. We then add peptides without structural representatives to this multiple sequence alignment by finding the most similar peptide with a structural representative, and performing pairwise sequence alignment on the two peptides (with no internal gaps).

Binding data were extracted from a total of 554 publications reporting domain-peptide binding assays. The complete training set is provided in Supplementary Data Set 2 (file includes PubMed ID of each publication).

**Implementation and Training**—All models were implemented in TensorFlow (v. 1.4). Learned parameters include the energetic terms comprising the Hamiltonian and a constant term, which approximates entropic contributions. The basis functions defined in HSM/D are learned and not pre-defined. In each training iteration, all domain families are represented. Consequently, the domain-specific weights receive gradients (only) from domain-peptide samples of the same class whereas the basis functions receive gradients from all domain families.

We used a  $k$ -fold cross-validation procedure ( $k = 8$ ). Data for each domain was randomly split into  $k$  independent subsets (folds). For each split, we hold out a single fold (“test data”) and re-train the model on the remaining folds (“training data”). Hyper-parameters ( $L^1$  regularization parameters per domain, number of epochs, learning rate) were fit against a randomly chosen training fold in a given split and a model was trained on the entire training set using these parameters. For novel prediction (*i.e.* for use in HSM/P), a model was re-trained on all training data with hyper-parameters averaged over all validation folds.

**Validation**—HSM/ID and HSM/D were first compared against position-specific scoring matrices (PSSMs). A PSSM,  $w$ , of length  $L$  is specified by an  $L \times A$  matrix ( $A$  is the number of amino-acids) where the  $l, a$ -th entry is the empirical probability of observing amino acid  $a$  at position  $l$ . The likelihood of observing a sequence  $s$  is then defined as:

$$P(s | w) = \prod_{i=1}^{|s|} P_i(s_i | w_i)$$

To compute this model, domains of a given class were clustered using average / unweighted pair group method with arithmetic mean (UPGMA)<sup>41</sup> with inter-sequence distance defined via the PAM120 substitution matrix. A PSSM was derived for each cluster from all the

empirical binding data in our training set. The clustering threshold was chosen to maximize the performance of the PSSMs on the test set.

Second, HSM/ID and HSM/D were compared with published models of PBD-peptide interactions if such models were available. The significance of the relative performance improvement of HSM/ID and MSM/D was assessed using the DeLong Test.<sup>42</sup>

## HSM/P

**Data**—We identified a total of 991 human PBDs in 591 proteins using the alignments constructed for HSM/D. For peptidic sites, tyrosine phosphosites were extracted from PhosphositePlus<sup>43</sup> and filtered to only include entries with a minimum of one literature citation. Potential non-phosphorylated sites (i.e. C-termini and polyproline sites) were selected based on two properties: solvent accessibility and disorder, which we predicted proteome-wide using RaptorX\_Property.<sup>44</sup> Using known ligands derived from the ELM<sup>45</sup> linear motif database, thresholds were chosen for RaptorX\_Property-predicted values to optimally recreate this known set of ligands. All C-termini regions (length = 6) that meet the previously described thresholds were included. Potential polyproline regions were identified by taking all protein regions that satisfied the previous thresholds and included at least one proline residue. At each proline, we search  $I$  residues in each direction ( $I = 8$ ). If a proline residue is encountered, that residue is added to the putative site, and the search is expanded by another  $I$  residues. If no proline residues are found, the site is padded by  $I/2$  in that direction. When no expansions are possible, the site is finalized as a potential polyproline binding site. This algorithm splits large regions (20+ residues) into subsets of contiguous prolines in a motif-agnostic way, i.e. a motif like ‘PxxP’ is not pre-defined.

Phosphosites and C-termini peptides were aligned in the same manner as described above for HSM training. For polyproline sites, all possible binding configurations were considered for a given site. That is, the bound ensemble represents the likelihood of a given domain binding the entire polyproline region. For efficiency, computation of PPIs only included ligands with greater than 0.01 probability of interaction.

The selection of peptidic sites represents a potential and unavoidable source of error. For example, some known ligands of SH3 (i.e. annotated via ELM) are excluded due to the solvent accessibility / disorder thresholds. The existence of annotation error necessarily informs interpretation of model results, as they are conditional on the space of selected ligands. We release the set of selected peptidic sites in our analysis (Supplementary Data Set 3) for future reference and possible improvement.

**Validation**—A high confidence set of PPIs, the “gold standard” set, was derived as follows. First, interaction data was extracted from the BioGRID<sup>29</sup> and IntAct<sup>30</sup> databases, which serve as repositories for experimentally-detected, manually curated PPI datasets. From these databases, all interactions were extracted that fit three criteria: (1) direct interaction (PSI-MI: 0407), (2) low-throughput source, and (3) reported by multiple (low-throughput) sources. Here, a low-throughput source is defined as any source reporting no more than 1,000 interactions. For comparative assessment, we used three recently released, high-throughput data sources: HT-MANN<sup>11</sup>, HT-GYGI (BioPlex)<sup>31,32</sup>, and HT-VIDAL<sup>33</sup>. Comparisons were

conducted on detectable interactions for each method (i.e. filtered based on bait-prey relationships). False-discovery rate (FDR) was based on literature-reported values for each source.<sup>33</sup> We report predictions at an equivalent FDR by combining HSM/D false-positive rates using Fisher's method (to derive a combined  $p$ -value) and correcting using the Benjamini-Hochberg method (see Fig. 2b).<sup>46</sup> For calculating HSM recall, we removed any PPIs in the gold standard set that may be comprised of domain-peptide interactions in the training set.

This benchmark likely underestimates the true predictive performance of HSM. While we only consider proteins that contain at least one PBD or peptidic site, we cannot guarantee that any given PPI will be PBD-mediated. The high-throughput methods considered can detect, in principle, any kind of PPI, unlike HSM which only predicts PBD-mediated ones. Furthermore, curated databases are primarily composed of higher-affinity PPIs<sup>1,34</sup>, presenting an underreporting bias against the types of PPIs HSM is specifically designed to predict.

As additional validation, we consider a set of chronologically-split PPIs reported in public repositories subsequent to when our (domain-level) training data was collected. Specifically, we combine all interactions from the three high-throughput proteomics experiments (HT-MANN, HT-GYGI, and HT-VIDAL) with all data reported in BioGRID following 2015 (IntAct does not record dates). We did not filter BioGRID using the previous three criteria as we wanted to maximize the number of PPIs for this analysis, but interactions reported prior to 2015 were removed. Predictions from HSM (FDR = 0.01) that confirmed these results are reported with the associated mechanisms visualized in Fig. 3 and Supplementary Fig. 4.

### Biophysical analysis of inferred models

Analyses of PBD-peptide co-complexes was performed by computing the Pearson correlation coefficient between all residue positions for a given PBD. We then summarize each position in the aligned PBD coordinate system by a set of second-order interaction energies  $(e_{i,j}^{(b)}(\alpha_i, \alpha_j))$ , where  $i$  and  $j$  correspond to residue positions in the PBD and peptide, respectively, and  $\alpha$  is the amino acid at a given position. We define the correlation between two PBD residue positions,  $m$  and  $n$ , as the correlation over all amino acid pairs and all peptide positions, i.e.:

$$r_{m,n}^{(D)} = \frac{\sum_{k=1}^{|P|} \sum_{\alpha_m, \alpha_k \in AA} (e_{m,k}^{(b)}(\alpha_m, \alpha_k) - \mu_m)(e_{n,k}^{(b)}(\alpha_n, \alpha_k) - \mu_n)}{\sqrt{\sum_{k=1}^{|P|} \sum_{\alpha_m, \alpha_k \in AA} (e_{m,k}^{(b)}(\alpha_m, \alpha_k) - \mu_m)^2} \sqrt{\sum_{k=1}^{|P|} \sum_{\alpha_n, \alpha_k \in AA} (e_{n,k}^{(b)}(\alpha_n, \alpha_k) - \mu_n)^2}}$$

This correlation coefficient effectively treats the similarity of different PBD residue positions as the average similarity of their inferred binding energies. Finally, we performed hierarchical clustering on all residue positions based on the above distance metric to order residue positions (clustering illustrated by a dendrogram; Fig. 4a). To enable visual inspection of energetically related surface patches, we associated colors with clusters using a greedy algorithm to map cophenetic distance into a color space.



Consider the set of non-singleton clusters,  $C_1, C_2, \dots, C_n$ , and singleton clusters,  $S_1, S_2, \dots, S_n$  that result from a given clustering threshold. For a given inter-cluster distance metric,  $\delta(\cdot, \cdot)$  (here, average / unweighted pair-group method with arithmetic mean (UPGMA)), we choose the next most distinct cluster,  $D_i = C_j$  on the basis of greatest sum of distances from the previously selected most distinct clusters,  $D_1, D_2, \dots, D_{i-1}$  (i.e.  $D_i = C_j$  if

$$C_j = \underset{C_k \notin D_1, \dots, D_{i-1}}{\operatorname{argmax}} \sum_{l=1}^{i-1} \delta(C_k, D_l)).$$

The first most distinct cluster,  $D_1$ , is chosen as the most distinct from all clusters. The first four clusters,  $D_1, D_2, D_3, D_4$ , are “anchored” into a color space by arbitrarily assigning the four “anchor colors” to the clusters. For each subsequent non-singleton cluster,  $D_i$ , we assign the red ( $R$ ), green ( $G$ ), and blue ( $B$ ) color channels by taking an inverse (cophenetic) distance weighted average of all previously colored channels (e.g. the fifth most distinct cluster is colored as a function of the first four clusters, the sixth as a function of the first five clusters, and so forth). For example, the red channel,  $R(\cdot)$ , of  $D_i$  is defined:

$$R(D_i) = \sum_{j=1}^{i-1} w_{D_i}(D_j) \cdot R(D_j)$$

where  $w_{D_i}(D_j)$  is defined as a basic inverse distance weight:

$$w_{D_i}(D_j) = \frac{\delta(D_i, D_j)^{-p}}{\sum_{j=1}^{i-1} \delta(D_i, D_j)^{-p}}$$

We found that setting  $p$  to 15 yielded the best results visually and emphasized nearby clusters. The green and blue channels are assigned in the same way. Singleton clusters were not assigned iteratively; rather, singletons were assigned as a mixture of all non-singleton clusters (i.e. all singletons are weighed with respect to the set  $C_1, C_2, \dots, C_n$ ). Colors were mapped onto representative co-complexes for which high resolution structures are available enabling identification of congruent surface patches (Fig. 4b–e; Supplementary Fig. 5–6).

Domain structures were also colored according to the interaction energy between domain and peptidic residues (Fig. 5). Using the second-order interaction energies  $e_{i,j}^{(b)}(\alpha_i, \alpha_j)$  ( $e_{i,j}^{(b)}(\alpha_i, \alpha_j)$ ), consider a domain residue at position  $i$ ,  $\alpha_i = a$ . The interaction energy is determined by the set of peptidic residues,  $p_1, p_2, \dots, p_n$ . We compute the total interaction energy is computed by averaging over all peptidic residues:

$$\bar{e}_i = \frac{1}{n} \sum_{j=1}^n e_{i,j}^{(b)}(a, p_j)$$

We may refine this average energy by considering subsets of peptidic residues that lie within a certain distance (we use radii of 2.5Å, 5Å, and 10Å) of the  $i$ -th domain position,  $\alpha_i$ . Residue-residue distance is defined by the closest pair of atoms in the domain and peptidic residues.

## Force-directed layout algorithm

Protein-protein interaction networks were laid out using a force-directed algorithm through the *graph-tool* Python package<sup>47</sup> (<https://graph-tool.skewed.de>). This algorithm simulates a pair of physical forces—repulsion between nodes (*i.e.* nodes are analogous to electrons) and springs for edges (*i.e.* all edges are approximately the same length). The layout results from minimizing the opposing forces (*i.e.* repulsion between nodes and attraction based on springs), placing nodes with similar sets of adjacent nodes close to one another. In the context of proteins, this translates into the formation of neighborhoods that have similar sets of neighboring proteins. The non-random structure of the networks shown in Figure 6 and Supplementary Figure 7 arises directly from these calculations and does not involve human intervention.

## Website

A Web-based tool was created to enable visualization of HSM interactions by capturing both topology and the PBD/peptide composition of individual nodes. At the review stage, the network can be viewed at (<https://ProteinPeptide.hms.harvard.edu>). A searchable interface is also provided to allow users to query for PPIs at varying likelihood thresholds.

## Reporting Summary

Further information on research design is available in the Reporting Summary linked to this article.

**DATA AVAILABILITY**—The domain-peptide and protein-protein interactions predictions are made available through a custom website (<https://ProteinPeptide.hms.harvard.edu>). The protein-peptide interaction data are also made available in figshare with the identifiers <https://doi.org/10.6084/m9.figshare.10084745>. Data used in training the model are available as Supplementary Data Set 2.

**CODE AVAILABILITY**—All code and data used for training and testing HSM are available in a public repository at <https://github.com/aqlaboratory/hsm>.

## Supplementary Material

Refer to Web version on PubMed Central for supplementary material.

## ACKNOWLEDGEMENTS

This work was funded by NIH Grants U54-CA225088 and P50-GM107618 and by DARPA/DOD grant W911NF-14-1-0397 to PKS.

## References

1. Gao A et al. Evolution of weak cooperative interactions for biological specificity. *Proc. Natl. Acad. Sci* 115, E11053–E11060 (2018). [PubMed: 30404915]
2. Perkins JR, Diboun I, Dessailly BH, Lees JG & Orengo C Transient Protein-Protein Interactions: Structural, Functional, and Network Properties. *Structure* 18, 1233–1243 (2010). [PubMed: 20947012]

3. Mayer BJ The discovery of modular binding domains: building blocks of cell signalling. *Nat. Rev. Mol. Cell Biol* 16, 691–698 (2015). [PubMed: 26420231]
4. Tompa P, Davey NE, Gibson TJ & Babu MM A Million Peptide Motifs for the Molecular Biologist. *Mol. Cell* 55, 161–169 (2014). [PubMed: 25038412]
5. Scott JD & Pawson T Cell Signaling in Space and Time: Where Proteins Come Together and When They're Apart. *Science* 326, 1220–1224 (2009). [PubMed: 19965465]
6. Cesareni G, Gimona M, Sudol M & Yaffe M Modular Protein Domains. (John Wiley & Sons, 2006).
7. Yang F et al. Protein Domain-Level Landscape of Cancer-Type-Specific Somatic Mutations. *PLOS Comput. Biol* 11, e1004147 (2015). [PubMed: 25794154]
8. Miller ML et al. Pan-Cancer Analysis of Mutation Hotspots in Protein Domains. *Cell Syst.* 1, 197–209 (2015). [PubMed: 27135912]
9. Rual J-F et al. Towards a proteome-scale map of the human protein–protein interaction network. *Nature* 437, 1173–1178 (2005). [PubMed: 16189514]
10. Beck M, Claassen M & Aebersold R Comprehensive proteomics. *Curr. Opin. Biotechnol* 22, 3–8 (2011). [PubMed: 20888217]
11. Hein MY et al. A Human Interactome in Three Quantitative Dimensions Organized by Stoichiometries and Abundances. *Cell* 163, 712–723 (2015). [PubMed: 26496610]
12. Levinson NM, Seeliger MA, Cole PA & Kuriyan J Structural Basis for the Recognition of c-Src by Its Inactivator Csk. *Cell* 134, 124–134 (2008). [PubMed: 18614016]
13. Waksman G, Shoelson SE, Pant N, Cowburn D & Kuriyan J Binding of a high affinity phosphotyrosyl peptide to the Src SH2 domain: Crystal structures of the complexed and peptide-free forms. *Cell* 72, 779–790 (1993). [PubMed: 7680960]
14. Demers J-P & Mittermaier A Binding Mechanism of an SH3 Domain Studied by NMR and ITC. *J. Am. Chem. Soc* 131, 4355–4367 (2009). [PubMed: 19267471]
15. Tinti M et al. The SH2 Domain Interaction Landscape. *Cell Rep.* 3, 1293–1305 (2013). [PubMed: 23545499]
16. Hou T, Chen K, McLaughlin WA, Lu B & Wang W Computational Analysis and Prediction of the Binding Motif and Protein Interacting Partners of the Abl SH3 Domain. *PLOS Comput. Biol* 2, e1 (2006). [PubMed: 16446784]
17. Kundu K, Mann M, Costa F & Backofen R MoDPepInt: an interactive web server for prediction of modular domain–peptide interactions. *Bioinformatics* 30, 2668–2669 (2014). [PubMed: 24872426]
18. Mignon D, Panel N, Chen X, Fuentes EJ & Simonson T Computational Design of the Tiam1 PDZ Domain and Its Ligand Binding. *J. Chem. Theory Comput* 13, 2271–2289 (2017). [PubMed: 28394603]
19. Kaneko T et al. Loops Govern SH2 Domain Specificity by Controlling Access to Binding Pockets. *Sci Signal* 3, ra34–ra34 (2010). [PubMed: 20442417]
20. AlQuraishi M, Koytiger G, Jenney A, MacBeath G & Sorger PK A multiscale statistical mechanical framework integrates biophysical and genomic data to assemble cancer networks. *Nat. Genet* 46, 1363–72 (2014). [PubMed: 25362484]
21. Zarrinpar A, Bhattacharyya RP & Lim WA The Structure and Function of Proline Recognition Domains. *Sci STKE* 2003, re8–re8 (2003). [PubMed: 12709533]
22. Denu JM & Dixon JE Protein tyrosine phosphatases: mechanisms of catalysis and regulation. *Curr. Opin. Chem. Biol* 2, 633–641 (1998). [PubMed: 9818190]
23. Wagner MJ, Stacey MM, Liu BA & Pawson T Molecular Mechanisms of SH2- and PTB-Domain-Containing Proteins in Receptor Tyrosine Kinase Signaling. *Cold Spring Harb. Perspect. Biol* 5, a008987 (2013). [PubMed: 24296166]
24. Harris BZ & Lim WA Mechanism and role of PDZ domains in signaling complex assembly. *J. Cell Sci* 114, 3219–3231 (2001). [PubMed: 11591811]
25. Kolodny R, Koehl P, Guibas L & Levitt M Small Libraries of Protein Fragments Model Native Protein Structures Accurately. *J. Mol. Biol* 323, 297–307 (2002). [PubMed: 12381322]
26. Nepomnyachiy S, Ben-Tal N & Kolodny R Global view of the protein universe. *Proc. Natl. Acad. Sci* 111, 11691–11696 (2014). [PubMed: 25071170]

27. Stormo GD, Schneider TD, Gold L & Ehrenfeucht A Use of the ‘Perceptron’ algorithm to distinguish translational initiation sites in *E. coli*. *Nucleic Acids Res.* 10, 2997–3011 (1982). [PubMed: 7048259]
28. Miller ML et al. Linear Motif Atlas for Phosphorylation-Dependent Signaling. *Sci Signal* 1, ra2–ra2 (2008). [PubMed: 18765831]
29. Chatr-aryamontri A et al. The BioGRID interaction database: 2017 update. *Nucleic Acids Res.* 45, D369–D379 (2017). [PubMed: 27980099]
30. Orchard S et al. The MIntAct project—IntAct as a common curation platform for 11 molecular interaction databases. *Nucleic Acids Res.* 42, D358–D363 (2014). [PubMed: 24234451]
31. Huttlin EL et al. The BioPlex Network: A Systematic Exploration of the Human Interactome. *Cell* 162, 425–440 (2015). [PubMed: 26186194]
32. Huttlin EL et al. Architecture of the human interactome defines protein communities and disease networks. *Nature* 545, 505–509 (2017). [PubMed: 28514442]
33. Rolland T et al. A Proteome-Scale Map of the Human Interactome Network. *Cell* 159, 1212–1226 (2014). [PubMed: 25416956]
34. Yoo J, Lee T-S, Choi B, Shon MJ & Yoon T-Y Observing Extremely Weak Protein–Protein Interactions with Conventional Single-Molecule Fluorescence Microscopy. *J. Am. Chem. Soc* 138, 14238–14241 (2016). [PubMed: 27758101]
35. Lee CH et al. A single amino acid in the SH3 domain of Hck determines its high affinity and specificity in binding to HIV-1 Nef protein. *EMBO J.* 14, 5006–5015 (1995). [PubMed: 7588629]
36. Fernandez-Ballester G, Blanes-Mira C & Serrano L The Tryptophan Switch: Changing Ligand-binding Specificity from Type I to Type II in SH3 Domains. *J. Mol. Biol* 335, 619–629 (2004). [PubMed: 14672668]
37. Schmidt H et al. Solution Structure of a Hck SH3 Domain Ligand Complex Reveals Novel Interaction Modes. *J. Mol. Biol* 365, 1517–1532 (2007). [PubMed: 17141806]
38. Teyra J et al. Comprehensive Analysis of the Human SH3 Domain Family Reveals a Wide Variety of Non-canonical Specificities. *Structure* 0, (2017).
39. Ma’ayan A et al. Formation of Regulatory Patterns During Signal Propagation in a Mammalian Cellular Network. *Science* 309, 1078–1083 (2005). [PubMed: 16099987]

## References (Online Methods-only)

40. Wilson D et al. SUPERFAMILY—sophisticated comparative genomics, data mining, visualization and phylogeny. *Nucleic Acids Res.* 37, D380–D386 (2009). [PubMed: 19036790]
41. Sokal RR & Michener CD A Statistical Methods for Evaluating Relationships. *Univ. Kans. Sci. Bull* 38, 1409–1448.
42. DeLong ER, DeLong DM & Clarke-Pearson DL Comparing the areas under two or more correlated receiver operating characteristic curves: a nonparametric approach. *Biometrics* 44, 837–845 (1988). [PubMed: 3203132]
43. Hornbeck PV et al. PhosphoSitePlus, 2014: mutations, PTMs and recalibrations. *Nucleic Acids Res.* 43, D512–D520 (2015). [PubMed: 25514926]
44. Peng J & Xu J Raptorx: Exploiting structure information for protein alignment by statistical inference. *Proteins Struct. Funct. Bioinforma* 79, 161–171 (2011).
45. Dinkel H et al. ELM—the database of eukaryotic linear motifs. *Nucleic Acids Res.* 40, D242–D251 (2012). [PubMed: 22110040]
46. Benjamini Y & Hochberg Y Controlling the False Discovery Rate: A Practical and Powerful Approach to Multiple Testing. *J. R. Stat. Soc. Ser. B Methodol* 57, 289–300 (1995).
47. Peixoto TP The graph-tool python library. (2017) doi:10.6084/m9.figshare.1164194.v14.

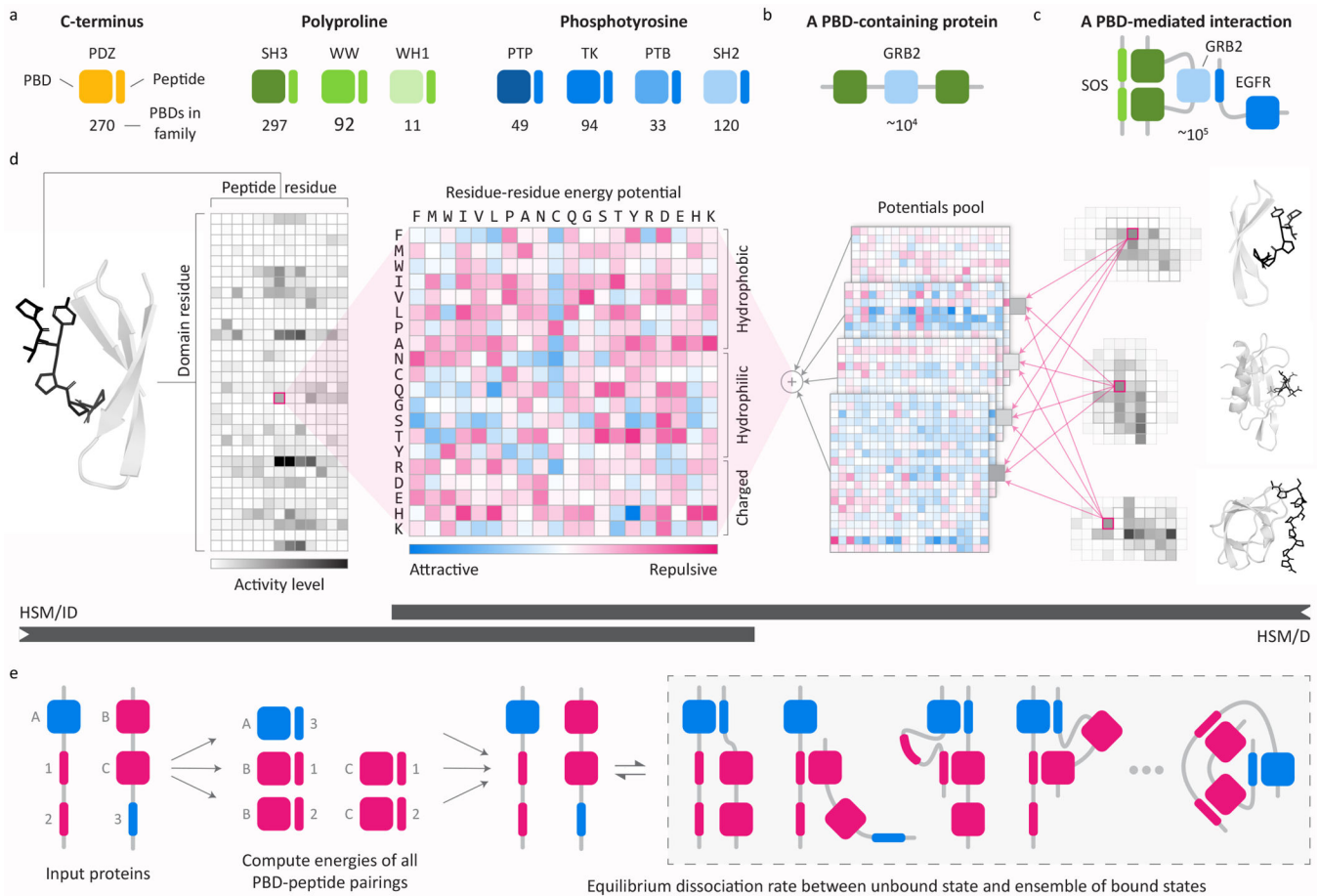


**Figure 1. Peptide-binding domains (PBDs) and modeling frameworks.**

(a-c) Schematic representations of the (a) PBD families modeled by HSM, (b) GRB2, a representative PBD-containing protein with one SH2 and two SH3 domains, and (c) a PBD-mediated ternary complex involving SOS, GRB2, and EGFR. The numbers of estimated (a) modeled human PBD domains, (b) PBD-containing proteins, and (c) interactions mediated by PBDs are shown below each schematic. (d) Two models of PBD-peptide interactions: HSM for independent domains (HSM/ID; left-to-right, model extent denoted by black bar) and HSM for domains (HSM/D, right-to-left). HSM/ID decomposes a PBD-peptide interaction into pairwise residue-residue interactions (grayscale matrix). Every pair of residue positions (one on the PBD, one on the peptide) within a PBD family is associated with a residue-residue energy potential (colored matrix, middle) that is machine-learned from data. Predictions for a given PBD/peptide combination are made by summing the energies associated with their amino acid sequences, then converting the summed energy into a probability. HSM/D learns a shared set of residue-residue potentials (overlapping colored matrices) across all position pairs and PBD families (grayscale matrix cutouts with associated structures, right). From this shared pool, a weighted mixture of potentials (grayscale blocks in “potentials pool”) is assigned to every position pair in every PBD family in a machine-learned fashion. Predictions are made by summing energies in the same way as for HSM/ID. (e) Multidentate PPIs are handled using the protein model (HSM/P) by predicting the energies of all possible PBD (A–C) and peptidic site (1–3) combinations

using HSM/D and then computing the equilibrium dissociation rate between the unbound state and the ensemble of all possible bound states (dashed gray box) using statistical mechanics techniques.



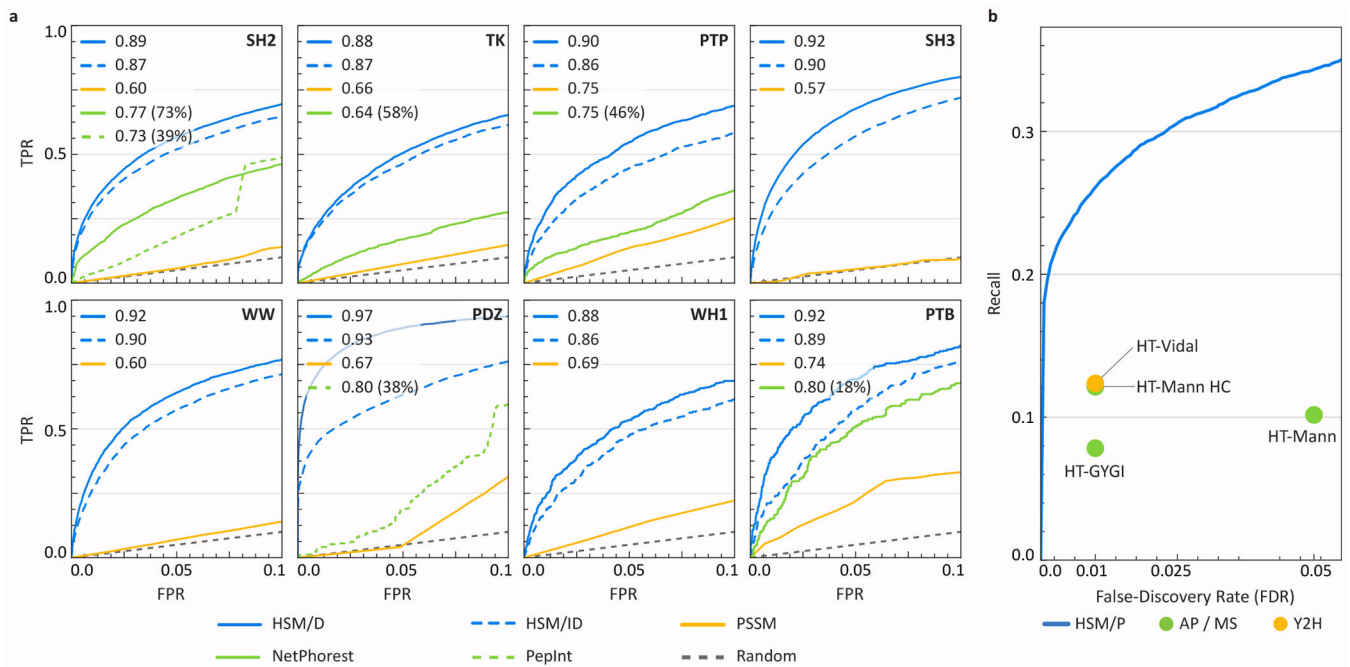


**Figure 2. Model performance and newly predicted PPIs.**

**(a)** Receiver operating characteristic (ROC) curves plotting the true positive rate (TPR) of HSM predictions and other methods as a function of the false positive rate (FPR) over a high-confidence region (FPR  $\leq$  0.1). Individual lines are labelled with the Area Under the ROC curve (AUROC) and the fraction of PBDs (in parentheses) covered by the method indicated relative to HSM. PSSM refers to Position-Specific Scoring Matrix<sup>27</sup>; NetPhorest<sup>28</sup> and PepInt<sup>17</sup> are collections of (independent) PBD models. AUROC is reported over the entire curve (i.e. over FPR ranging from 0 to 1). The complete ROC curves are plotted in Supplementary Figure 3a. **(b)** Recall vs. false discovery rate (FDR) of physically-validated PPIs (*e.g.* by isothermal titration calorimetry;  $n = 32,504$  interactions; see Methods) for HSM/P (blue curve) and for two affinity purification/mass spectrometry datasets, (AP/MS) HT-GYGI<sup>31,32</sup> and HT-MANN/HT-MANN High-Confidence (HT-MANN HC;<sup>11</sup> green points; Supplementary Table 5) and one yeast two-hybrid (Y2H; orange point) dataset, HT-VIDAL<sup>33</sup>.

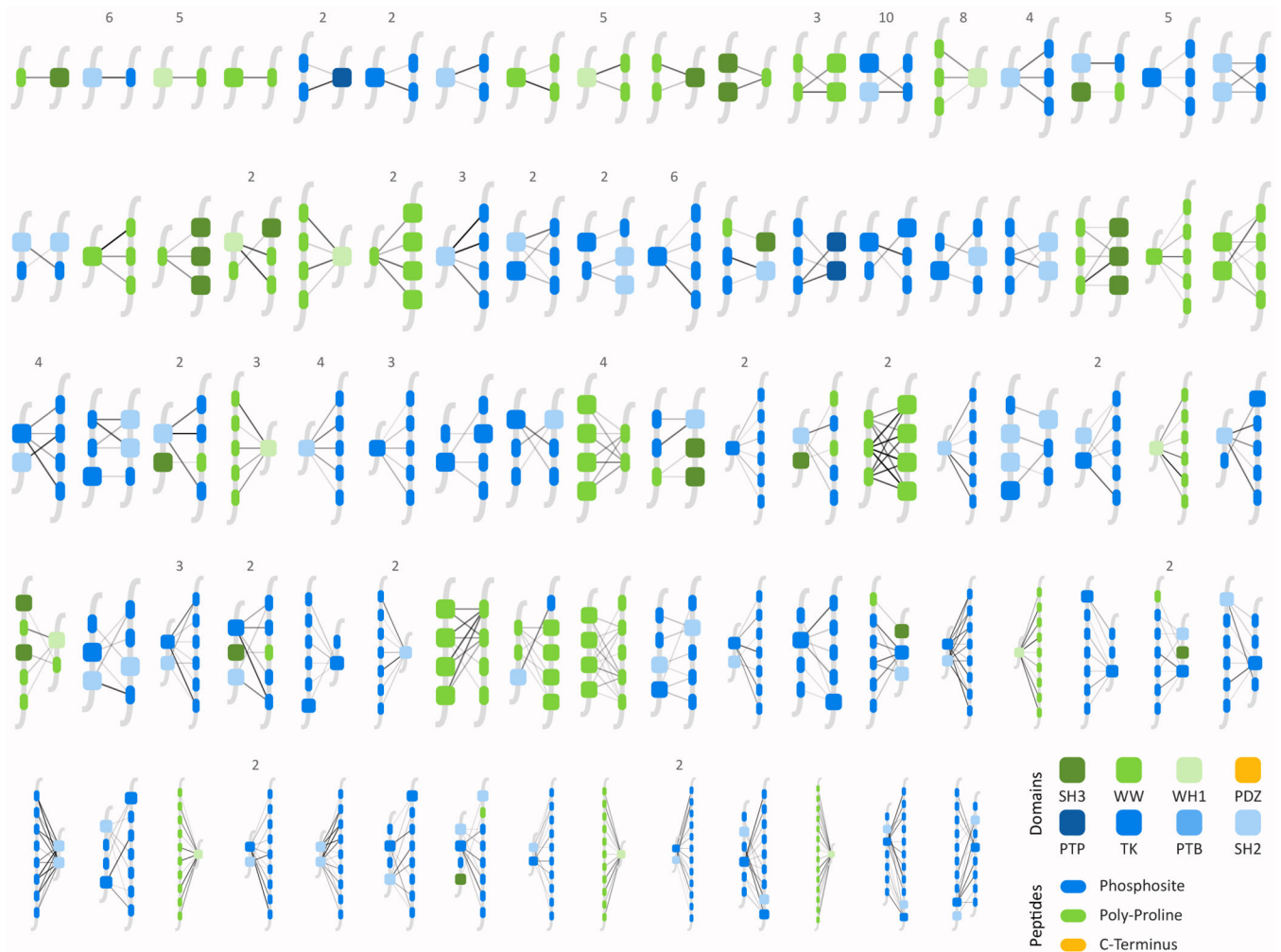


### Figure 3. Predicted mechanisms for newly predicted interactions.

Schematics of PBD-peptide interactions driving 161 newly reported PPIs as predicted by HSM/P. Numbers denote how many examples of each PBD/peptide configuration were identified. The complete set of annotated interaction mechanisms is shown in Supplementary Fig. 4. PBD-peptide interaction strength is denoted by edge opacity. Experimental data confirming these interactions were obtained from BioGRID<sup>29</sup> (n = 37), HT-VIDAL (n = 31), HT-MANN (n = 32) and HT-GYGI (n = 86). No PDZ-mediated interactions were observed, likely owing to experimental bias: the attachment of a tag to the C-terminus of a protein, necessary for affinity purification, disrupts PDZ-mediated interactions.

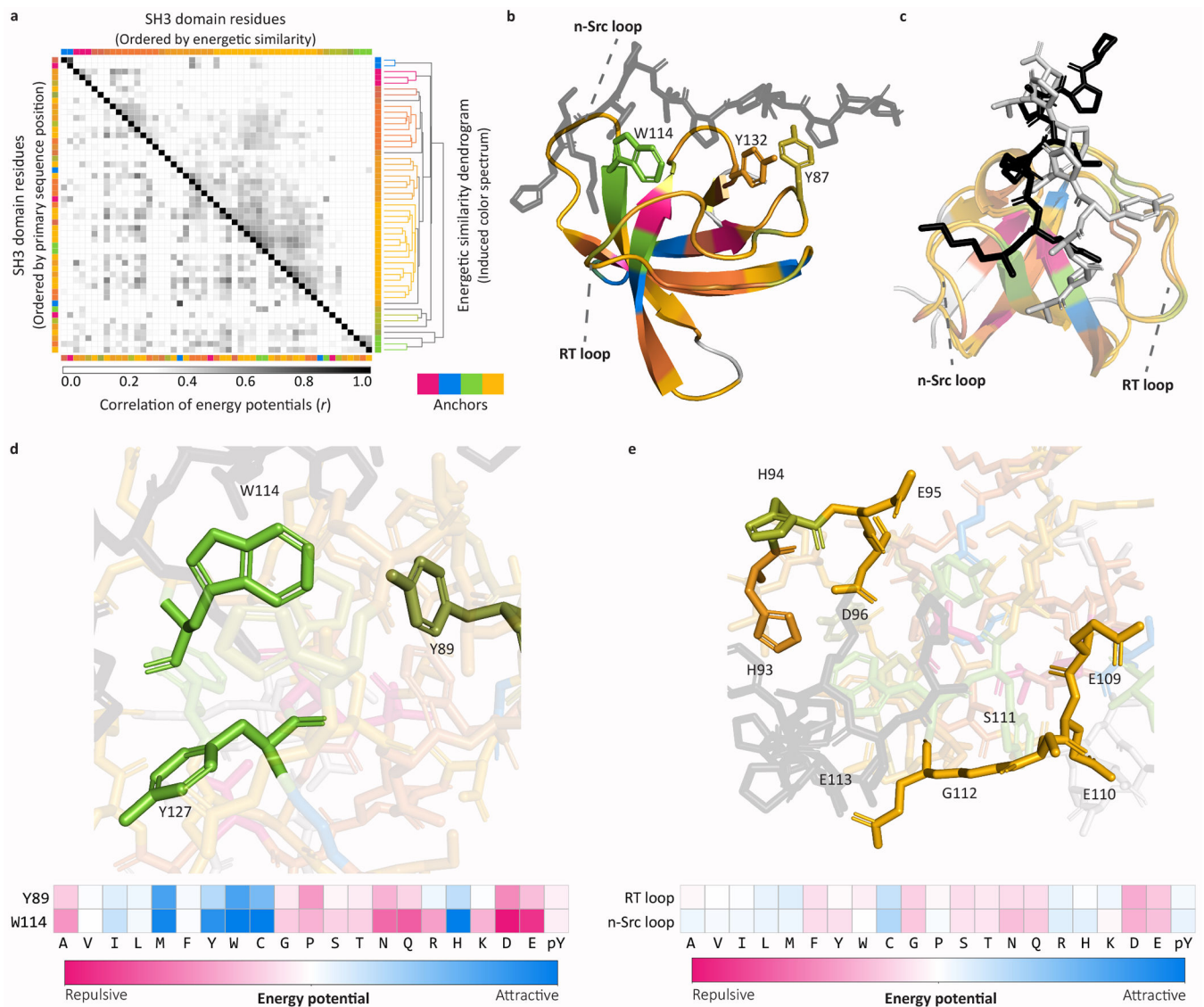


**Figure 4. Mechanistic analysis of SH3 domain binding.**

(a) Correlation matrix of energy potentials at every residue position in the SH3 domain model. Correlation (Pearson's  $r$ ,  $n = 7,056$  energies comprising each domain residue - peptide potential (21 amino acids  $\times$  21 amino acids  $\times$  16 peptide residue positions)) level is shown in grayscale. Lower-left half of the matrix is ordered by sequence position. Upper-right half of the matrix is ordered by bi-clustering distance (shown as a dendrogram). Colors (top, right) are assigned based on cophenetic distance (see text) and mapped to the sequence (bottom, left). (b) Structure of the HCK SH3 domain in complex with a bound peptide (black; PDB accession code 2OI3). Domain residues are color coded based on the clustering patterns shown in panel (a). The aromatic triplet residues in the HCK SH3 domain (Y87, W114, Y132) and specificity-defining loops (RT, n-Src) are labeled. (c) Overlaid SH3-peptide co-complexes (PDB accession codes 1FYN, 1CKA) highlighting the conformational flexibility of bound peptides between the n-Src and RT-loops. SH3 domains are colored using the energetic color spectrum from panel (a). Peptides are highlighted in black (1CKA)

and white (1FYN). **(d)** Close-up of the SH3 tryptophan switch (W114) and energetically-related residues (Y89, Y127). HSM infers a similar energetic profile (similar colors) for W114 and the spatially adjacent residues Y89 (shared functional similarity with Y87-associated cluster) and Y127. This energetic similarity implies a common functional role for this triplet that is complementary to the role played by three previously recognized canonical aromatic residues (Y87, W114, Y132). Energy potentials for the interaction of W114 and Y89 with a single peptide position (bottom) show strong energetic concordance. **(e)** Close-up of the RT (top) and n-Src (bottom) loops exhibit a set of energetically similar, acidic residues, supporting peptidic conformational flexibility. Mean HSM energy potentials for each loop are shown below.



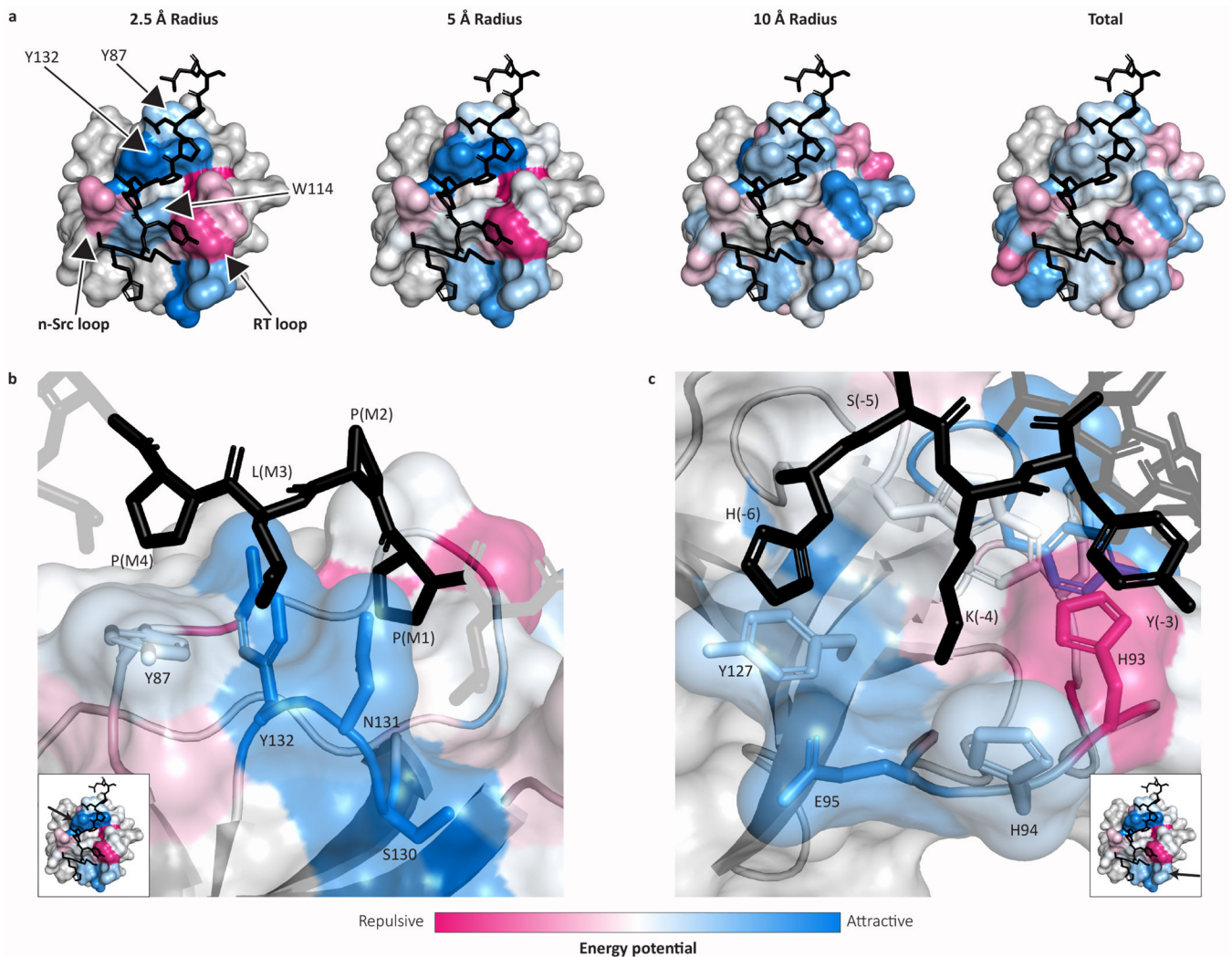


**Figure 5 |. Energy surface of SH3-peptide co-complex.**

(a) Energy surfaces for the interaction between the SH3 domain of HCK and a peptide with the sequence HSKYLPPLPSL. Each SH3 residue is colored with its mean predicted energy of interaction with peptidic residues lying within a specified distance (2.5Å, 5Å, 10Å; residue-residue distances are measured between the closest pair of atoms) and with all peptidic residues (“Total”; not bounded by a distance). (b-c) Close-up view of energy surfaces for <math><5\text{\AA}</math> interactions. Position and orientation are indicated by arrows on inset structures. (b) Close-up of the core proline-binding motif (Y87, Y132) along with adjacent residues (S130, N131) that interact with the peptide proline motif (HSKYLPPLPSL). Motif positions are denoted by ‘Mx’ where x is the position within the motif in the N-to-C orientation. (c) Close-up of the specificity defining RT-loop in the SH3 domain with the N-terminal region of the bound peptide (HSKYLPPLPSL). An adjacent SH3 residue, Y127 (on the  $\beta$ -sheet), is included in the highlighted residues.

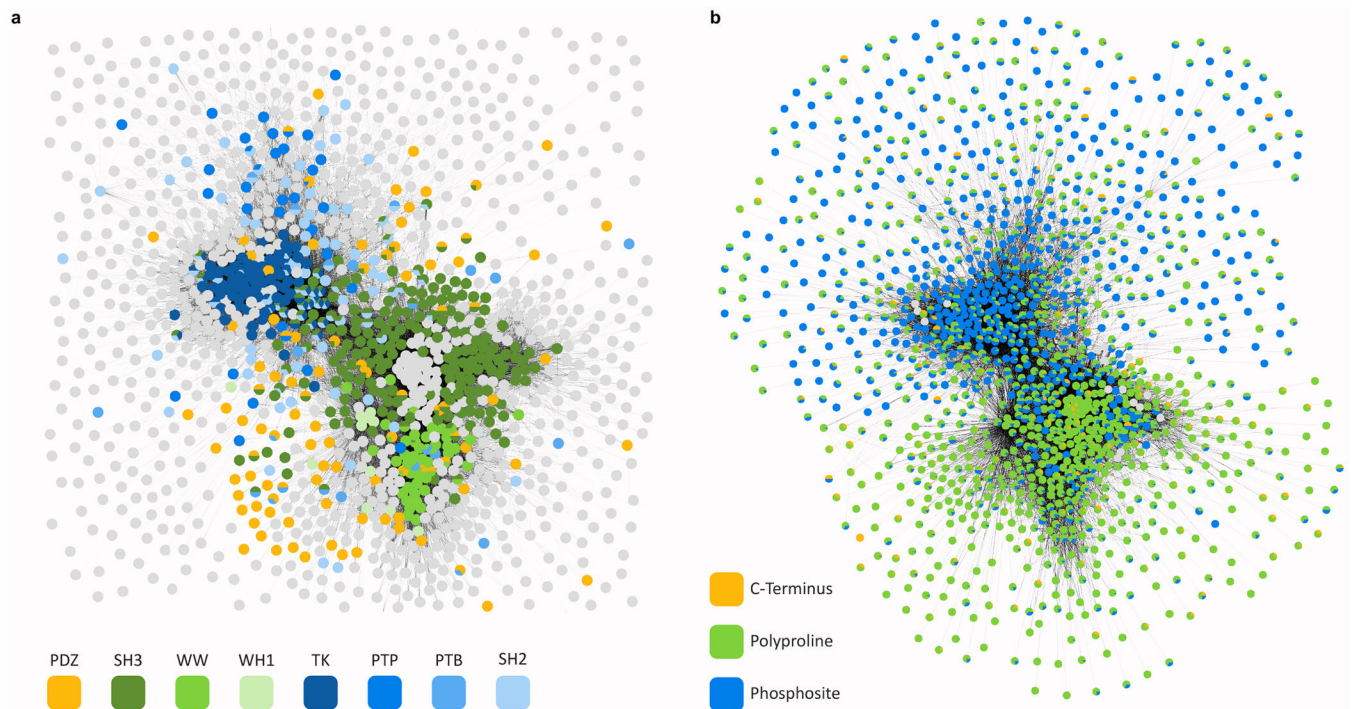


**Figure 6 | Hierarchical organization of the human PBD-mediated PPI network.**

**(a-b)** Human PPI network with nodes corresponding to proteins and edges to predicted interactions (HSM/P,  $p > 0.7$ ). Nodes were automatically laid out using a force-directed layout. Each node is represented by a pie chart that denotes **(a)** domain or **(b)** peptidic site composition. Blue denotes phosphotyrosine-associated mechanisms, green, proline-associated mechanisms, orange, C-terminus-associated mechanisms, and white, no-associated mechanisms (i.e. a protein that contains no modeled PBDs in **(a)**). For visualization, maximal adjacency for each node is limited to the 50 most probable partners. (See Supplementary Fig. 7 for networks per PBD family; see [website](#) for higher quality images)